Diastolic Dysfunction in a Pre-clinical Model of Diabetes Is Associated With Changes in the Cardiac Non-myocyte Cellular Composition

Charles D. Cohen
Baker Heart and Diabetes Institute
Miles J. De Blasio
Monash University MIPS: Monash Institute of Pharmaceutical Sciences
Man K. S. Lee
Baker Heart and Diabetes Institute
Gabriella E. Farrugia
Baker Heart and Diabetes Institute
Darnel Prakoso
Monash University MIPS: Monash Institute of Pharmaceutical Sciences
Crisdion Krstevski
Baker Heart and Diabetes Institute
Minh Deo
Monash University MIPS: Monash Institute of Pharmaceutical Sciences
Daniel G. Donner
Baker Heart and Diabetes Institute
Helen Kiriazis
Baker Heart and Diabetes Institute
Michelle C. Flynn
Baker Heart and Diabetes Institute
Taylah L. Gaynor
Baker Heart and Diabetes Institute
Andrew J. Murphy
Baker Heart and Diabetes Institute
Grant R. Drummond
Baker Heart and Diabetes Institute
Alexander R. Pinto
Baker Heart and Diabetes Institute
Rebecca Helen Ritchie (rebecca.ritchie@monash.edu)
Monash University MIPS: Monash Institute of Pharmaceutical Sciences https://orcid.org/0000-0002-8610-0058

Research Article

Keywords: Cardiac cellularity, diabetes, flow cytometry, echocardiography, fibroblast

DOI: https://doi.org/10.21203/rs.3.rs-342544/v1

Abstract

Background:

Diabetes is associated with a significantly elevated risk of cardiovascular disease and its specific pathophysiology remains unclear. Recent studies have changed our understanding of cardiac cellularity, with cellular changes accompanying diabetes yet to be examined in detail. This study aims to characterise the changes in the cardiac cellular landscape in murine diabetes to identify potential cellular protagonists in the diabetic heart.

Methods:

Diabetes was induced in male FVB/N mice by low-dose streptozotocin and a high-fat diet for 26-weeks. Cardiac function was measured by echocardiography at endpoint. Flow cytometry was performed on cardiac ventricles as well as blood, spleen, liver, and bone-marrow at endpoint from non-diabetic and diabetic mice. To validate flow cytometry results, immunofluorescence staining was conducted on left-ventricles of age-matched mice.

Results

Mice with diabetes exhibited hyperglycaemia and impaired glucose tolerance at endpoint. Echocardiography revealed reduced E:A and e':a' ratios in diabetic mice indicating diastolic dysfunction. Systolic function was not different between the experimental groups. Detailed examination of cardiac cellularity found resident mesenchymal cells (RMCs) were elevated as a result of diabetes, due to a marked increase in cardiac fibroblasts, while smooth muscle cells were reduced in proportion. Moreover, we found increased levels of Ly6C^{hi} monocytes in both the heart and in the blood. Consistent with this, the proportion of bone-marrow haematopoietic stem cells were increased in diabetic mice.

Conclusions:

Murine diabetes results in distinct changes in cardiac cellularity. These changes—in particular increased levels of fibroblasts—offer a framework for understanding how cardiac cellularity changes in diabetes. The results also point to new cellular mechanisms in this context, which may further aid in development of pharmacotherapies to allay the progression of cardiomyopathy associated with diabetes.

Background

Diabetes mellitus is a leading cause of death worldwide, with a total global prevalence exceeding 450 million individuals [1]. In 2015, diabetes was attributed to 12.8% of total all-cause mortality worldwide, providing a substantial socioeconomic burden and health concern [2, 3].

Diabetes is associated with a significantly elevated risk of cardiovascular death and hospitalisation for heart failure (HF) [4, 5]. However, there remains no specific treatment for HF or its development in

individuals with diabetes. HF in diabetes is often accompanied by impaired cardiac output, cardiac fibrosis, cardiomyocyte hypertrophy, cell death, and oxidative stress [6]. Diabetes also involves chronic and systemic inflammation [7, 8] with monocytosis and neutrophilia [7–9]. Despite extensive efforts to characterise diabetes-induced HF, inherent cellular mechanisms underpinning cardiac dysfunction in diabetes remain to be ascertained.

The mammalian heart consists of a diverse range of cell types [10]. Cardiac non-myocytes—comprised of endothelial cells (ECs), resident mesenchymal cells (RMCs) and leukocytes—outnumber myocytes, and are critical for maintaining homeostasis of the heart [10, 11]. While a number of recent studies have provided valuable new insight into the disparate roles of non-myocytes in cardiac homeostasis [10, 12] and pathological remodelling [13–15], the cellular dynamics of non-myocytes during development of diabetes-induced heart failure remains unexplored. Using a recently published murine model of diabetes-induced cardiomyopathy [16], this study aimed to determine the difference in cardiac non-myocyte cellular proportions compared to non-diabetic mice. Here, we show that experimental diabetes impacts multiple cellular compartments in the heart, providing a framework for understanding the cellular dynamics and mechanisms driving development of diabetes-induced heart failure.

Research Design And Methods

Animal experiments

All animal-related experiments were approved by the Alfred Research Alliance (ARA) Animal Ethics Committee (Ethics number: E/1681/2016/B) and were performed in accordance with the National Health and Medical Research Council of Australia. FVB/N mice were sourced from the ARA Animal Services (provided in three separate cohorts). Mice had access to food and water *ad libitum* and were housed at 22°C on a 12 h light/dark cycle. Male 6-week-old FVB/N mice were randomly allocated into the non-diabetic (ND, n=7) citrate vehicle control group fed standard chow diet, or diabetes mellitus (diabetes, n=19) which was induced by the combination of low-dose streptozotocin (STZ; cat# AG-CN2-0046, AdipoGen Life Sciences, NSW, Australia) and high-fat-diet (HFD; SF04-001, Specialty Feeds, WA, Australia, 43% total calculated digestible energy from lipids). STZ was administered by three consecutive daily intraperitoneal (i.p.) injections (55mg/kg body weight in 0.1mol/L citric acid vehicle, pH 4.5 [cat# 251275, Sigma-Aldrich, USA]). Mice administered STZ were subsequently fed a HFD *ad libitum* for 26-weeks, as previously described [16]. Blood glucose levels were measured fortnightly via saphenous vein bleeds using a glucometer (Accu-Chek® Performa II, Roche Diagnostics, NSW, Australia). Intraperitoneal glucose and insulin tolerance tests were conducted at endpoint (26-weeks of diabetes) to assess glucose clearance and insulin resistance, as previously described [16]. Whole-body composition analysis was performed at endpoint using an Echo-MRI™ 4-in-1 700 Analyser (EchoMRI, Houston, TX, USA) to assess percentage fat mass and total lean mass. Percentage glycated haemoglobin (% HbA_{1c}) was also measured at endpoint to assess long-term blood glucose levels (Cobas b 101 POC system, Roche Diagnostics, NSW, Australia). Mice were euthanised by administration of Ketamine/Xylazine (85/8.5mg/kg, i.p.) and subsequent cardiac exsanguination. As previously described [10–12], the thoracic

cavity was exposed and right atrium was cut to allow for cardiac perfusion through the left-ventricular apex (PBS, 0.9mM $CaCl_2$, 200mM KCl), after which the heart was excised and ventricles were used for flow cytometry.

Echocardiography

Echocardiography was conducted in mice under anaesthesia (Ketamine/Xylazine/Atropine [KXA], 80/8/0.96mg/kg, i.p.) at 26-weeks post diabetes (32-weeks of age) using a Philips iE33 ultrasound machine with a 15-MHz linear-array transducer. Analysis was conducted at the Baker Heart and Diabetes Institute and quality control was completed by technicians at the Preclinical Cardiology Microsurgery & Imaging Platform (PCMIP). Doppler flow echocardiography was used to assess cardiac transmitral flow velocity in each phase of diastole, where the early phase (E wave) and the late phase (A wave) were measured to determine the E:A ratio. Similarly, tissue Doppler was performed to examine the tissue motion of the mitral annulus (early phase = e', late phase = a' wave). M-mode echocardiography was conducted to assess left ventricle (LV) systolic function. Variables obtained from M-mode analysis included LV end-diastolic dimension (LVEDD) and LV end-systolic dimension (LVESD) to calculate fractional shortening (%FS = [(LVEDD-LVESD)/LVEDD] × 100).

Flow cytometry

Blood, spleen and bone marrow

Whole blood was obtained by cardiac puncture at endpoint and stained using a leukocyte-specific antibody panel (Supplementary Table 3). Bone marrow from the tibia and femur were flushed using PBS without Mg^{2+} and Ca^{2+} into 50mL centrifuge tubes. Spleens were manually dissociated and passed through a 35μM filter into 50mL centrifuge tubes to obtain a single cell suspension as previously described [7]. Blood, spleen and bone marrow were then subjected to red blood cell (RBC) lysis for 15 minutes at 4°C using an ammonium chloride based commercial lysis buffer (1X dilution, 555899, Becton Dickinson, USA). After RBC lysis, the remaining stained cells were washed twice in 'Fx buffer' (1 X HBSS [Gibco™, NY, USA], 2% FCS). Between each wash, cells were centrifuged at 400×*g* for 5 minutes at 4°C. Cells were then resuspended in 200μl of Fx buffer containing 4',6-diamidino-2-phenylindole (DAPI [0.1μg/mL]); and filtered through 35μM mesh into 5ml polystyrene round-bottom tubes (352052, Falcon®, NY, USA) for flow cytometry. Gating strategies for each of the above cell suspensions are provided in Supplementary Figures 3-5. For normalisation of flow cytometry data, 20μl of blood was used to measure total white blood cell count using a Sysmex XS-1000i Hematology Analyzer.

Heart

High-dimensional flow-cytometry was performed on cardiac ventricles (comprising the LV, ventricular septum and right ventricle) from ND and mice with diabetes. Following perfusion, hearts were minced using curved scissors (14077-09, Walton, USA) as previously described [10], and transferred to 5ml microfuge tubes for enzymatic digestion at 37°C (2 mg/mL collagenase type IV [LS004188, Worthington

Biochem, NJ, USA], 1 mg/mL Dispase II [04942078001, Roche, NSW, Australia] in 0.9 mM $CaCl_2$ in PBS). Cardiac non-myocyte cells were triturated three times at 15-minute intervals using a Pasteur pipette to mechanically aid enzymatic digestion for a total of 45 minutes. Digested non-myocyte cardiac cells were then filtered through 75μM nylon mesh into a 15mL tube containing 10 mL of cold PBS (0.9 mM $CaCl_2$) and subjected to centrifugation (200*g*, 15 minutes, 4°C – no breaks) for debris clearance. The majority of the supernatant was aspirated and the remaining volume (~1 mL) was washed with a further 1 mL of Fx buffer supplemented with 0.9 mM $CaCl_2$. Cells were pelleted at 400×*g* (4 minutes, 4°C) and resuspended in 200μl of Fx Buffer with Ca^{2+} to yield the single cell suspension of non-myocyte cardiac cells. Cells were then stained using the antibody panel designed for examining the non-myocyte fraction of the heart (Supplementary Table 4). Cells were strained through a 35μm filter and flow cytometry was performed on a BD LSR Fortessa™ X-20 Special Order system located at the Baker Heart and Diabetes Institute.

Histological analysis

Age and sex-matched, fresh-frozen LV samples embedded in Optimal Cutting Temperature (OCT) compound were acquired from a separate cohort of ND and mice with diabetes [16] for histological analysis. LV sections were cut (10μm) on a cryostat (CM1950, Leica Biosystems) for staining (ND: n = 11, diabetes: n = 11). LV sections were co-stained with GATA4 (1:100, 14-9980-80, eBioScience™, Invitrogen, Australia) and PCM1 (1:100, 19856-1-AP, Proteintech Group, USA) antibodies to delineate the cell abundance of RMCs ($PCM1^-GATA4^+$ cells) as recently reported [12]. Serial sections were stained with DACH1 (1:100, 10914-1-AP, ProteinTech, USA) to quantify EC abundance [10, 12]. All immunofluorescence sections were counterstained with DAPI to identify total cell nuclei. Immunofluorescence micrographs of each LV sample were acquired at a 20X objective and tiled (3x3 fields of view) on a Nikon A1R confocal laser scanning microscope. Quantified values of immunofluorescence signal were normalised to total nuclei ($DAPI^+$).

Statistical analysis

Flow cytometry data was analysed using FlowJo (v10.7.1) software. Raw cardiac flow cytometry data was normalised to the mean of the ND values within each batch, such that the mean of each ND cell type is equal to 1. Raw blood flow cytometry data was normalised to total white-blood cell count obtained from the hematology analyser, then subsequently batch normalised as aforementioned. Immunofluorescence micrographs were analysed by QuPath software (v0.2.3), using the cell count function to quantify nuclei. Echocardiography data was analysed using RadiAnt DICOM viewer software (v2020.2), after which quantification was performed in accordance with the PCMIP guidelines. All data was illustrated and analysed statistically using Graphpad Prism (v8.1.2). Comparison of experimental groups was conducted using an unpaired *t*-test, whereby statistical significance was determined as $P < 0.05$.

Results

The STZ-HFD model recapitulates primary features of diabetes

The presence of diabetes was confirmed by a range of physiological tests prior to euthanasia. Consistent with our previous report [16], mice with diabetes exhibited significantly elevated blood glucose at endpoint (Supplementary Table 1). This was corroborated by measurement of glycated haemoglobin (% HbA_{1c}) at endpoint, which was significantly increased in mice with diabetes ($P < 0.0001$; Supplementary Table 1). In this study however, mice exhibiting diabetes did not gain more weight than their ND counterparts (Supplementary Table 1). This was recapitulated by the EchoMRI body composition analysis, showing no differences in lean or fat mass (Supplementary Table 1) between experimental groups. Impaired glucose tolerance was evident in mice with diabetes, indicating reduced clearing efficiency of systemic glucose, presented as the area under the curve (AUC, $P < 0.0001$, Supplementary Table 1). In contrast, there was no difference in the AUC from the insulin tolerance test between ND and mice with diabetes (Supplementary Table 1).

STZ-HFD mice exhibit LV diastolic dysfunction, but not systolic dysfunction

Echocardiography measurements of LV diastolic and systolic function were recorded *in vivo*, to determine the degree of cardiac functional impairment in mice with diabetes relative to their ND counterparts. Pulsed-wave Doppler echocardiography was conducted to measure mitral blood flow velocity during the early (E-wave) and late (A-wave) filling phases of diastole (Supplementary Figure 1A). Heart rate (HR) tended to be elevated in mice with diabetes, but this did not reach statistical significance ($P=0.07$; Supplementary Figure 1B). Although no differences were detected in the peak E wave (Supplementary Figure 1C), the peak A wave velocity was significantly elevated in mice with diabetes compared to ND mice ($P < 0.05$; Supplementary Figure 1D). Consequently, a significant reduction in E:A ratio (a hallmark feature of diastolic dysfunction) was observed in diabetic hearts vs. ND ($P < 0.05$ Supplementary Figure 1E). There were no differences in other measurements of diastolic function including deceleration time or isovolumic relaxation time (IVRT) between experimental groups (Supplementary Figure 1F, 1G, respectively).

To accompany transmitral blood flow, tissue Doppler echocardiography was used to assess the velocity of the mitral valve itself in each phase of diastole (e' = early phase, a' late phase, Supplementary Figure 1H-L). Although the peak e' velocity was only modestly reduced ($P = 0.054$, Supplementary Figure 1I) and the peak a' velocity exhibited a minor increase ($P = 0.072$, Supplementary Figure 1J), the e':a' ratio was significantly lower in mice with diabetes compared to ND mice ($P < 0.05$, Supplementary Figure 1K). There were no detectable changes in the E:e' ratio between cohorts (Supplementary Figure 1L).

M-Mode echocardiography was also performed to assess the difference in ventricular wall thickness and systolic function in mice with diabetes. The anterior wall thickness at diastole (AWd), LV end-diastolic dimension (LVEDD) and posterior wall thickness at diastole (PWd) were not different between groups (Supplementary Table 2). Surprisingly, fractional shortening (% FS) was significantly elevated in mice

with diabetes compared with ND mice ($P < 0.05$; Supplementary Table 2), which is likely explained by the minor increase in LV end-systolic dimension in diabetic hearts (LVESD; $P = 0.07$, Supplementary Table 2).

Diabetes alters the cardiac non-myocyte cellular composition

To assess differences in cardiac cellularity associated with diabetes-induced HF, we performed flow cytometric analysis of murine cardiac ventricles at study endpoint. Examination of metabolically active, viable single-cells (Supplementary Figure 2) revealed significant differences in the proportion of endothelial cells (ECs; 0.26-fold decrease) and resident mesenchymal cells (RMCs; 2-fold increase) indicating diabetes alters cardiac cellularity (Figure 1A-B). Conversely, leukocytes were at similar levels in ND and mice with diabetes (Figure 1A-B).

Next, we sought to validate the shifts in EC and RMC populations in diabetes observed by flow cytometry, with immunohistochemical analysis (Figure 1C-D). To achieve this, we stained left ventricular sections of both cohorts with an antibody cocktail of GATA4 and PCM1 (Figure 1C) or DACH1 (Figure 1D), which we have previously employed to quantify proportions of RMCs and ECs [12]. These analyses revealed that RMC ($PCM1^{-}GATA4^{+}$) cell counts were significantly elevated in diabetic heart sections compared to ND counterparts ($P < 0.05$, Figure 1C). Using the same approach for ECs, serial sections stained with DACH1 indicated no differences in EC abundance between experimental groups (Figure 1D), suggesting that the proportional difference observed by flow cytometry is driven by the increased RMCs.

Considering the proportion of RMCs were markedly elevated in the diabetic heart, a range of RMC subtypes were investigated from the initial RMC gate (Supplementary Figure 2). Fibroblasts were significantly increased in diabetic hearts compared to ND (2.36-fold, $P < 0.0001$, Figure 2B). In contrast, the proportion of smooth muscle cells (SMCs), were reduced in the diabetic cohort compared to ND controls (0.27-fold, $P < 0.05$, Figure 2B). No major changes were observed in total mural cells, pericyte or Schwann cell populations (Figure 2B).

While we did not detect any changes in total resident leukocyte proportions in diabetic mouse hearts compared to ND (Figure 1B), diabetes has been previously associated with cardiac inflammation and systemic monocytosis [7, 17, 18]. To develop an overview of leukocyte diversity and abundance in diabetic hearts, we identified an array of leukocytes including myeloid and lymphoid cell populations and their subsets (Figure 3A). There were no differences in cardiac leukocyte subsets between cohorts, except $Ly6C^{hi}$ monocytes, which were significantly increased in the myocardium of mice with diabetes (1.8-fold, Figure 3B).

Circulating $Ly6C^{hi}$ monocytes are elevated in diabetes

To confirm systemic monocytosis, we quantified circulating leukocytes and their broad subtypes by flow cytometry. As shown previously [7][19][16], monocytes, particularly the $Ly6C^{hi}$ subset, were significantly elevated in the blood of mice with diabetes (2.2-fold, 2.3-fold, respectively; $P < 0.05$ for both; Figure 4B). Numbers of circulating neutrophils and $Ly6C^{lo}$ monocytes were also marginally elevated in diabetic mice

compared to their ND counterparts ($P = 0.09$, $P = 0.054$ respectively; Figure 4B,). By contrast, numbers of circulating lymphocytes (B and T-cells) did not differ between cohorts (Figure 4C).

Systemic monocytosis likely occurs via extramedullary myelopoiesis

To identify the potential sources of the observed monocytosis in this model, we performed flow cytometry of the bone marrow and spleen. Within the bone marrow, LSKs (haematopoietic stem and progenitor cells; [$Lin^{-}Sca1^{+}cKit^{+}$]) were significantly increased in mice with diabetes (1.8-fold, $P < 0.01$, Figure 5A). However, bone-marrow derived common myeloid progenitors (CMP) and granulocyte-myeloid progenitors (GMP) were not different between experimental groups (Figure 5A). Monocytes (both $Ly6C^{hi}$ and $Ly6C^{lo}$) were significantly increased in the spleen in mice with diabetes compared to their ND controls (1.7-fold, 1.3-fold respectively, $P < 0.05$, Figure 5B). These data suggest that the increased proportion of bone-marrow LSKs could be influencing these cells to mobilise to the spleen to undergo extramedullary myelopoiesis (Figure 5C).

Discussion

The relationship between diabetes and HF remains poorly understood. Diabetes-associated cardiac remodelling— encompassing myocyte hypertrophy, fibrosis, oxidative stress and apoptosis [13, 14] is well established. However, how the cardiac non-myocyte networks change in diabetes and contribute to this remodelling is unclear. Using a recently characterised mouse model of diabetes-induced cardiomyopathy [20], we aimed to determine how diabetes affects cardiac non-myocyte proportions and abundance. We revealed that with diabetes-associated diastolic dysfunction, proportions of cardiac fibroblasts are significantly increased in the myocardium. We also noted increased levels of $Ly6C^{hi}$ monocytes and decreased levels of SMCs in diabetic hearts.

Numerous studies have implicated cardiac fibroblasts in diabetic cardiomyopathy, however their precise role in diabetes *in vivo* is still unknown. Cardiac fibroblasts are the primary cell type involved in deposition of extracellular matrix (ECM) in both states of acute injury or chronic stress [21]. However, in these contexts, fibroblast gene expression and phenotype are distinct [13]. For example, in myocardial infarction (MI), fibroblasts rapidly differentiate into activated fibroblasts and myofibroblasts—both well-established drivers of cardiac ECM deposition [16, 22, 23]. Conversely, we have recently reported that myofibroblasts are absent during the development of chronic fibrosis in angiotensin II-induced cardiac remodelling [24, 25]. Observations from the present study reveal that fibroblasts are the predominant non-myocyte cell type most dramatically affected by diabetes—suggesting an important role for fibroblasts in the development of diabetes-induced HF. Indeed, chronic hyperglycaemia is known to up-regulate various pro-fibrotic genes in the diabetic heart as a whole, including *Col1a1, Postn, Timp-2* and *Ccn2* [26]. Furthermore, diabetes is associated with fibroblast-to-myofibroblast differentiation and ECM deposition [7, 8]. However, further research such as single-cell sequencing or targeted cell depletion experiments are needed to further elucidate the precise role of the cardiac fibroblast in diabetes and the regulatory mechanisms that drive these changes.

In the current study, we also observed an increase in monocyte numbers in the heart in diabetic mice, which is likely the result of increased systemic inflammation. In the non-injured heart, circulating leukocytes, such as monocytes primarily reside in the vascular lumens of cardiac capillaries [27–29], therefore reflecting changes occurring in the circulation. Systemic monocytosis is reported in both type-1 diabetes (T1D) and insulin resistant obese mice (i.e. leptin mutant *ob/ob* mice and diet-induced obese mice) [30]. Consistent with systemic inflammation, the diabetic heart exhibits upregulation of pro-inflammatory cytokines such as TNFα, MCP-1 and IL-1β [7, 8]. Corresponding to the monocytosis, we also noted increased progenitor cells and splenic monocytes—the major site of secondary myelopoiesis [31]. Monocytosis is a well-established feature of diabetes and obesity/insulin resistance [32, 33]. However, in this model we only detected a significant increase in haematopoietic stem and progenitor cells (HSPCs), but not common myeloid progenitors (CMPs) or granulocyte-macrophage progenitors (GMPs) in the bone marrow. Given HSPCs can migrate to secondary myelopoietic sites, such as the spleen, to increase monocyte numbers [34, 35], our findings suggest that this may be the primary mode of monocytosis observed in our model (Figure 5C).

In contrast to the diabetes-induced increases in cardiac fibroblasts and monocyte numbers, we observed a decrease in SMC proportions. This was unexpected given hyperglycaemia has previously been associated with inhibition of aortic vascular SMC apoptosis in T1D patients, and in STZ-induced T1D mice [36–38]. Conversely, metabolic syndrome and hypercholesterolaemia are both associated with increased apoptosis in aortic VSMCs of mice and humans [39, 40]. Therefore, the precise mechanism leading to the reduction in SMC proportions in the hearts of STZ-HFD mice warrants further investigation.

Although there are a number of studies examining the role of individual cardiac cell types in diabetes, to our knowledge this is the first study to consider the entire cardiac non-myocyte network to understand differences in tissue cellularity. While novel technologies such as single-cell RNA sequencing have been successfully applied to tissues such as the pancreas [41], kidney [13, 42] and liver [43, 44] in diabetes, detailed interrogation of the cellular heterogeneity in these tissue systems are lacking in this context. This study invites future research to consider cellular plasticity in diabetes to better understand the development of its associated pathologies.

Study Limitations

While this study provides a basis for providing new understanding of the cardiac cellular dynamics in the context of diabetes, a number of limitations are noteworthy. First, cardiomyocytes were not considered in this study, as they are too large in diameter to pass through the flow cytometer available in our laboratories. Although cardiomyocytes are detectable by histology ($PCM1^{+}GATA4^{+}$ cells), they are often multi-nucleated, thus counting nuclei abundance is unlikely to yield accurate information. Second, we only examined male mice in our study. Given that cardiac pathology is sex-specific in mice [11, 12] and in humans [16, 45], cardiac cellular composition and gene expression are sexually-dimorphic [46]. Future work should examine the impact of biological sex in the development of diabetic cardiomyopathy. Third, the STZ-HFD model used in this study did not yield a population of mice with elevated fat mass and body

weight as expected [47, 48]. Adiposity and obesity are important comorbidities contributing to pathology in experimental and clinical T2D [46], albeit obesity is not essential for development of T2D [47, 48]. Importantly however, in this study mice with diabetes exhibited hyperglycaemia, impaired glucose tolerance and LV diastolic dysfunction, which are clinically relevant features of HF associated with diabetes. Lastly, we were unable to ascertain whether the observed differences are attributed to the combination of STZ and HFD, or one of these individual insults. Further work using this model should consider the effect of STZ and HFD alone in addition to the combination of STZ-HFD to delineate the role of both factors in the development of diabetic HF.

Conclusion

Here we have profiled the differences in the cardiac non-myocyte network, observing that the cellular landscape of the heart changes in a murine model of diabetes. These results offer a framework for understanding the cellular mechanisms that may drive pathological remodelling of the heart during the development of diabetes-induced HF. Targeting the molecular pathways that drive these non-myocyte cellular changes may offer new therapeutic avenues to address the cardiac complications associated with diabetes.

Declarations

Acknowledgements

We wish to acknowledge the Monash Micro-Imaging (MMI) facility for provision of instrumentation and training.

Disclosures

None.

Data availability

The datasets used and/or analysed during the current study are available from the corresponding author on reasonable request.

Author contributions

CDC, MJD, RHR, ARP, conceived the experiments, GD, MJD, AJM and MKSL provided intellectual input. CDC, ARP, MJD, GEF, CK, TLG, MCF, DP, MD performed experiments. HK, DD performed echocardiography imaging and assisted with quality control of echocardiography analysis. CDC wrote the manuscript under ARP and RHR's guidance. RHR, ARP, MJD, GD edited the manuscript. All co-authors read and approved the final manuscript.

Funding

CDC, CK and TLG are supported by the La Trobe University Postgraduate Research Scholarship (LTUPRS), Research Training Program Fees Off-set (RTP-Fo) Scholarship. CDC is supported by a Baker Institute ‘Bright Sparks’ Scholarship. TLG is supported by Defence Science Institute (DSI) RhD Grant. This work was supported by a project grant to RHR and MJD from the National Health and Medical Research Council (NHMRC) of Australia (APP1158013), and an NHMRC fellowship to RHR (APP1059960) and in part by an infrastructure grant from the Victorian Government of Australia. This work was also supported by an NHMRC Ideas Grant (GNT1188503) to ARP.

Competing interests

None.

Ethics approval

All animal-related experiments were approved by the Alfred Research Alliance (ARA) Animal Ethics Committee (Ethics number: E/1681/2016/B) and were in accordance with NHMRC guidelines.

Consent for publication

Not applicable.

References

1. Raghavan S, Vassy JL, Ho YL, Song RJ, Gagnon DR, Cho K, et al. Diabetes mellitus–related all-cause and cardiovascular mortality in a national cohort of adults. Journal of the American Heart Association. 2019;8.
2. Ng ACT, Delgado V, Borlaug BA, Bax JJ. Diabesity: the combined burden of obesity and diabetes on heart disease and the role of imaging. Nature Reviews Cardiology. 2020.
3. Ogurtsova K, da Rocha Fernandes JD, Huang Y, Linnenkamp U, Guariguata L, Cho NH, et al. IDF Diabetes Atlas: Global estimates for the prevalence of diabetes for 2015 and 2040. Diabetes Research and Clinical Practice. 2017;128:40–50.
4. Petar M, Mark C, Gerasimos S, Stefan D, Walter J, Boer D, et al. Type 2 diabetes mellitus and heart failure : a position statement from the Heart Failure Association of the European Society of Cardiology Type 2 diabetes mellitus and heart failure : a position statement from the Heart Failure Association of the European. 2018;20:853–72.
5. Rubler S, Dlugash J, Yuceoglu YZ, Kumral T, Branwood AW, Grishman A. New type of cardiomyopathy associated with diabetic glomerulosclerosis. The American Journal of Cardiology. 1972;30:595–602.
6. Ritchie RH, Dale Abel E. Basic mechanisms of diabetic heart disease. Circulation Research. 2020;126:1501–25.

7. Nagareddy PR, Murphy AJ, Stirzaker RA, Hu Y, Yu S, Miller RG, et al. Hyperglycemia promotes myelopoiesis and impairs the resolution of atherosclerosis. Cell Metabolism. 2013;17:695–708.
8. Nagareddy PR, Kraakman M, Masters SL, Stirzaker RA, Gorman DJ, Grant RW, et al. Adipose tissue macrophages promote myelopoiesis and monocytosis in obesity. Cell Metabolism. 2014;19:821–35.
9. Wong SL, Demers M, Martinod K, Gallant M, Wang Y, Goldfine AB, et al. Diabetes primes neutrophils to undergo NETosis, which impairs wound healing. Nature Medicine. 2015;21:815–9.
10. Pinto AR, Ilinykh A, Ivey MJ, Kuwabara JT, D'Antoni ML, Debuque R, et al. Revisiting cardiac cellular composition. Circulation Research. 2016;118:400–9.
11. Skelly DA, Squiers GT, Mclellan MA, Bolisetty MT, Robson P, Rosenthal NA, et al. Single-cell transcriptional profiling reveals cellular diversity and intercommunication in the mouse heart. Cell Reports. 2018;22:600–10.
12. Squiers GT, Mclellan MA, Ilinykh A, Branca J, Rosenthal NA, Pinto AR. Cardiac cellularity is dependent upon biological sex and is regulated by gonadal hormones. Cardiovascular Research. 2020;cva265:1–25.
13. McLellan MA, Skelly DA, Dona MSI, Squiers GT, Farrugia GE, Gaynor TL, et al. High-resolution transcriptomic profiling of the heart during chronic stress reveals cellular drivers of cardiac fibrosis and hypertrophy. Circulation. 2020;142:1448–63.
14. Forte E, Skelly DA, Chen M, Daigle S, Morelli KA, Hon O, et al. Dynamic interstitial cell response during myocardial infarction predicts resilience to rupture in genetically diverse mice. Cell Reports. 2020;30:3149-3163.e6.
15. Farbehi N, Patrick R, Dorison A, Xaymardan M, Janbandhu V, Wystub-Lis K, et al. Single-cell expression profiling reveals dynamic flux of cardiac stromal, vascular and immune cells in health and injury. eLife. 2019;8:1–39.
16. Tate M, Prakoso D, Willis AM, Peng C, Deo M, Qin CX, et al. Characterising an alternative murine model of diabetic cardiomyopathy. Frontiers in Physiology. 2019;10:1–15.
17. Westermann D, Rutschow S, Jäger S, Linderer A, Anker S, Riad A, et al. Contributions of inflammation and cardiac matrix metalloproteinase activity to cardiac failure in diabetic cardiomyopathy: The role of angiotensin type 1 receptor antagonism. Diabetes. 2007;56:641–6.
18. Chu PY, Walder K, Horlock D, Williams D, Nelson E, Byrne M, et al. CXCR4 antagonism attenuates the development of diabetic cardiac fibrosis. PLoS ONE. 2015;10:1–13.
19. Huynh K, Bernardo BC, McMullen JR, Ritchie RH. Diabetic cardiomyopathy: Mechanisms and new treatment strategies targeting antioxidant signaling pathways. Pharmacology and Therapeutics. 2014;142:375–415.
20. Tallquist MD, Molkentin JD. Redefining the identity of cardiac fibroblasts. Nature Reviews Cardiology. 2017;14:484–91.
21. Krstevski C, Cohen CD, Dona MSI, Pinto AR. New perspectives of the cardiac cellular landscape: mapping cellular mediators of cardiac fibrosis using single-cell transcriptomics. Biochemical Society Transactions. 2020;48:2483–93.

22. Hutchinson KR, Lord CK, West TA, Stewart JA. Cardiac fibroblast-dependent extracellular matrix accumulation is associated with diastolic stiffness in type-2 diabetes. PLoS ONE. 2013;8.
23. Prakoso D, De Blasio MJ, Qin C, Rosli S, Kiriazis H, Qian H, et al. Phosphoinositide 3-kinase (p110α) gene delivery limits diabetes-induced cardiac NADPH oxidase and cardiomyopathy in a mouse model with established diastolic dysfunction. Clinical science. 2017;131:1345–60.
24. Fowlkes V, Clark J, Fix C, Law BA, Morales MO, Qiao X, et al. Type II diabetes promotes a myofibroblast phenotype in cardiac fibroblasts. Life Sciences. 2013;92:669–76.
25. Sedgwick B, Riches K, Bageghni SA, O'Regan DJ, Porter KE, Turner NA. Investigating inherent functional differences between human cardiac fibroblasts cultured from nondiabetic and type 2 diabetic donors. Cardiovascular Pathology. 2014;23:204–10.
26. Epelman S, Lavine KJ, Randolph GJ. Origin and functions of tissue macrophages. Immunity. 2014;41:21–35.
27. Qin CX, Finlayson SB, Al-Sharea A, Tate M, De Blasio MJ, Deo M, et al. Endogenous Annexin-A1 regulates haematopoietic stem cell mobilisation and inflammatory response post myocardial infarction in mice in vivo. Scientific Reports. 2017;7.
28. Kassan M, Choi SK, Galán M, Bishop A, Umezawa K, Trebak M, et al. Enhanced NF-κB activity impairs vascular function through PARP-1-, SP-1-, and COX-2-dependent mechanisms in type 2 diabetes. Diabetes. 2013;62:2078–87.
29. Jadhav A, Tiwari S, Lee P, Ndisang JF. The heme oxygenase system selectively enhances the anti-inflammatory macrophage-M2 phenotype, reduces pericardial adiposity, and ameliorated cardiac injury in diabetic cardiomyopathy in Zucker diabetic fatty rats. Journal of Pharmacology and Experimental Therapeutics. 2013;345:239–49.
30. Swirski FK, Nahrendorf M. Leukocyte behavior in atherosclerosis, myocardial infarction, and heart failure. Science. 2013;339:161–6.
31. Dutta P, Hoyer FF, Grigoryeva LS, Sager HB, Leuschner F, Courties G, et al. Macrophages retain hematopoietic stem cells in the spleen via VCAM-1. Journal of Experimental Medicine. 2015;212:497–512.
32. Ruiz E, Gordillo-Moscoso A, Padilla E, Redondo S, Rodriguez E, Reguillo F, et al. Human vascular smooth muscle cells from diabetic patients are resistant to induced apoptosis due to high Bcl-2 expression. Diabetes. 2006;55:1243–51.
33. Hall JL, Matter CM, Wang X, Gibbons GH. Hyperglycemia inhibits vascular smooth muscle cell apoptosis through a protein kinase C-dependent pathway. Circulation Research. 2000;87:574–80.
34. Clarke MCH, Figg N, Maguire JJ, Davenport AP, Goddard M, Littlewood TD, et al. Apoptosis of vascular smooth muscle cells induces features of plaque vulnerability in atherosclerosis. Nature Medicine. 2006;12:1075–80.
35. Martínez-Hervás S, Vinué Á, Núñez L, Andrés-Blasco I, Piqueras L, TomásReal J, et al. Insulin resistance aggravates atherosclerosis by reducing vascular smooth muscle cell survival and increasing CX3CL1/CX3CR1 axis. Cardiovascular Research. 2014;103:324–36.

36. Segerstolpe Å, Palasantza A, Eliasson P, Andersson EM, Andréasson AC, Sun X, et al. Single-cell transcriptome profiling of human pancreatic islets in health and type 2 diabetes. Cell Metabolism. 2016;24:593–607.
37. Wang YJ, Schug J, Won KJ, Liu C, Naji A, Avrahami D, et al. Single-cell transcriptomics of the human endocrine pancreas. Diabetes. 2016;65:3028–38.
38. Rai V, Quang DX, Erdos MR, Cusanovich DA, Daza RM, Narisu N, et al. Single-cell ATAC-Seq in human pancreatic islets and deep learning upscaling of rare cells reveals cell-specific type 2 diabetes regulatory signatures. Molecular Metabolism. 2020;32:109–21.
39. Fu J, Akat KM, Sun Z, Zhang W, Schlondorff D, Liu Z, et al. Single-cell RNA profiling of glomerular cells shows dynamic changes in experimental diabetic kidney disease. Journal of the American Society of Nephrology. 2019;30:533–45.
40. Wilson PC, Wu H, Kirita Y, Uchimura K, Ledru N, Rennke HG, et al. The single-cell transcriptomic landscape of early human diabetic nephropathy. Proceedings of the National Academy of Sciences of the United States of America. 2019;116:19619–25.
41. Xiong X, Kuang H, Ansari S, Liu T, Gong J, Wang S, et al. Landscape of intercellular crosstalk in healthy and NASH liver revealed by single-cell secretome gene analysis. Molecular Cell. 2019;75:644-660.e5.
42. Alex L, Russo I, Holoborodko V, Frangogiannis NG. Characterization of a mouse model of obesity-related fibrotic cardiomyopathy that recapitulates features of human heart failure with preserved ejection fraction. The American Journal of Physiology-Heart and Circulatory Physiology. 2018;315:H934–49.
43. Beale AL, Meyer PMD, Marwick TH, Lam CSP, Kaye DM. Sex differences in cardiovascular pathophysiology why women are overrepresented in heart failure with preserved ejection fraction. Circulation. 2018;138:198–205.
44. Cheng S, Xanthakis V, Sullivan LM, Lieb W, Massaro J, Aragam J, et al. Correlates of echocardiographic indices of cardiac remodeling over the adult life course: Longitudinal observations from the framingham heart study. Circulation. 2010;122:570–8.
45. Prakoso D, De Blasio MJ, Tate M, Kiriazis H, Donner DG, Qian H, et al. Gene therapy targeting cardiac phosphoinositide 3-kinase (p110α) attenuates cardiac remodeling in type 2 diabetes. American Journal of Physiology - Heart and Circulatory Physiology. 2020;318:H840–52.
46. Kahn SE, Cooper ME, del Prato S. Pathophysiology and treatment of type 2 diabetes: Perspectives on the past, present, and future. The Lancet. 2014;383:1068–83.
47. Yoon K-H, Lee J-H, Kim J-W, Cho JH, Choi Y-H, Ko S-H, et al. Epidemic obesity and type 2 diabetes in Asia. The Lancet. 2006;368:1681–8.
48. George AM, Jacob AG, Fogelfeld L. Lean diabetes mellitus: An emerging entity in the era of obesity. World Journal of Diabetes. 2015;6:613.

Figures

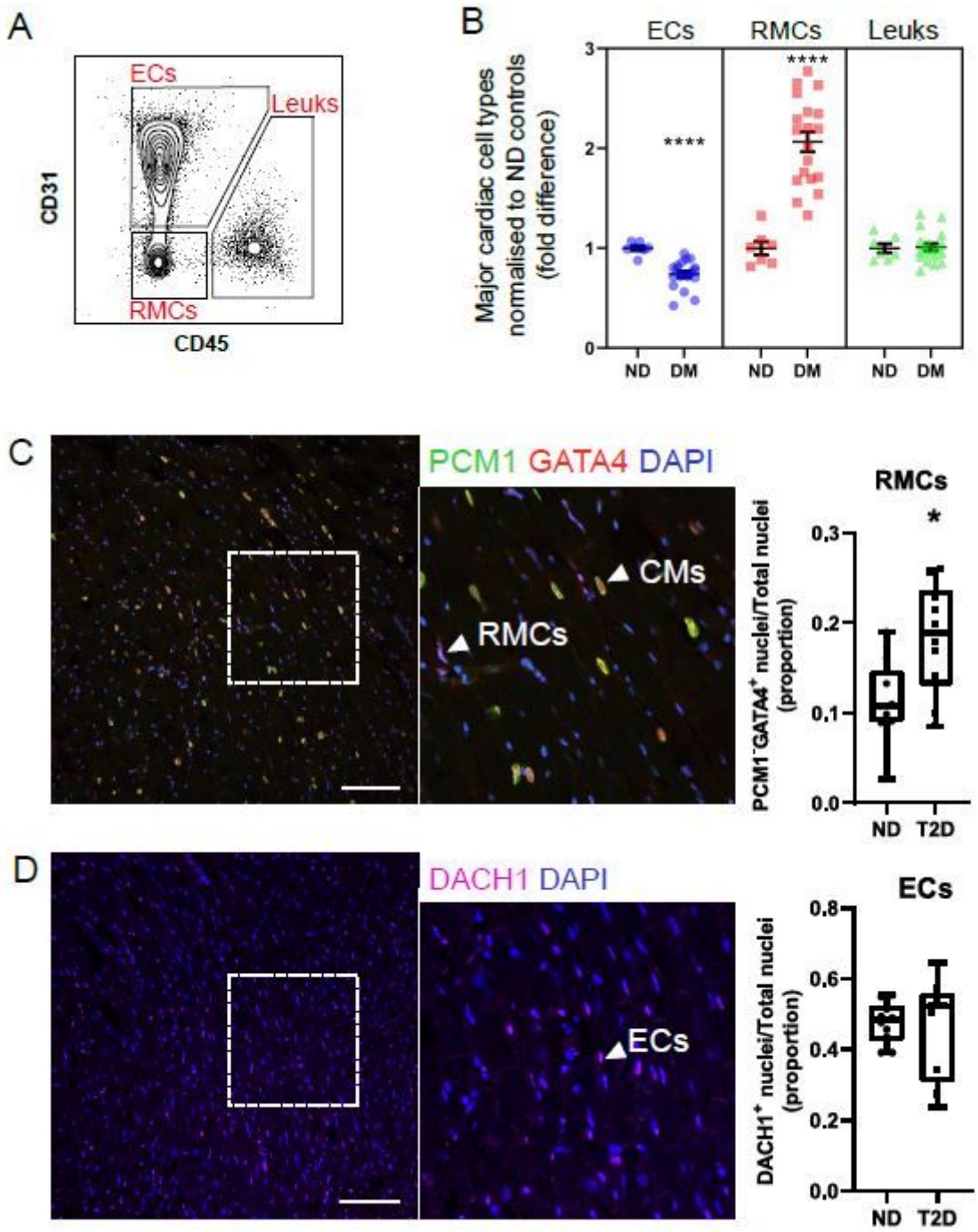

Figure 1

Differences in the abundance of major non-myocyte cell classes in the diabetic heart. (A) Flow cytometry contour plot displaying gating of major non-myocyte cell types for quantification of cell type proportion (summarised in B). For full gating strategy see Supplementary Figure 2. Endothelial cells (ECs; CD31+), resident mesenchymal cells (RMCs; CD31-CD45-) and leukocytes (Leuks; CD45+). (B) Proportions of major cell types in non-diabetic (ND; n = 7) and diabetic (T2D; n = 19) mouse hearts. Individual sample values are shown with mean ± SEM. (C) Immunohistochemical analysis of the abundance of RMCs in ND

and diabetic mouse heart left ventricles. Left and middle panels show representative confocal micrographs of mouse heart tissue stained for PCM1 and GATA4. PCM1+GATA4+ and PCM1 GATA4+ nuclei correspond to nuclei of cardiomyocytes (CM) and RMCs respectively. Nuclei are counterstained with DAPI. Right panel (box-plot) summarises proportion of nuclei corresponding to RMCs in ND (n = 9) vs. T2D (n = 10) enumerated from micrographs. Whiskers of box-and-whisker plot indicate max and min. (D) As for C, heart left ventricle sections were stained with Dach1 to identify nuclei corresponding to endothelial cells in ND (n = 10) and T2D (n = 9) left ventricles. *P < 0.05, **** P < 0.0001 (Student's unpaired t-test). Scale bar = 100μM.

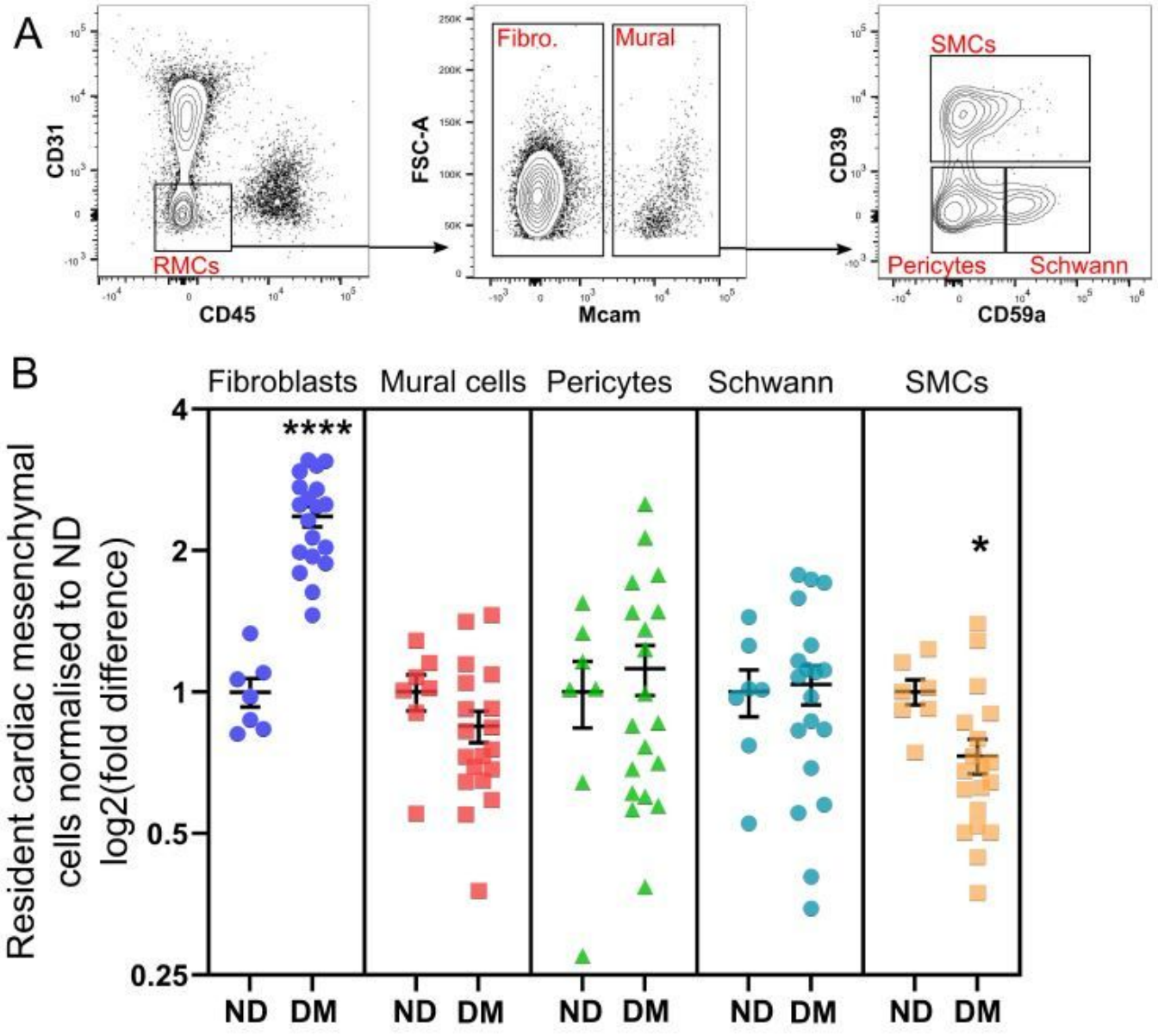

Figure 2

Differences in resident mesenchymal cell (RMC) subtypes in the diabetic heart. (A) Flow cytometry contour plots display gating strategy for cardiac RMCs and subsets (fibroblasts, SMCs, pericytes and Schwann cells) for quantifying RMC proportions (summarised in B). For full gating strategy see Supplementary Figure 2. (B) Proportions of RMC sub-classes in ND (n = 7) and diabetic (n = 19) mouse ventricles. Fibro: Fibroblast; Mural: Mural cells; SMCs: smooth muscle cells. Data is displayed as mean ± SEM. *P < 0.05, **** P < 0.0001 (Student's unpaired t-test).

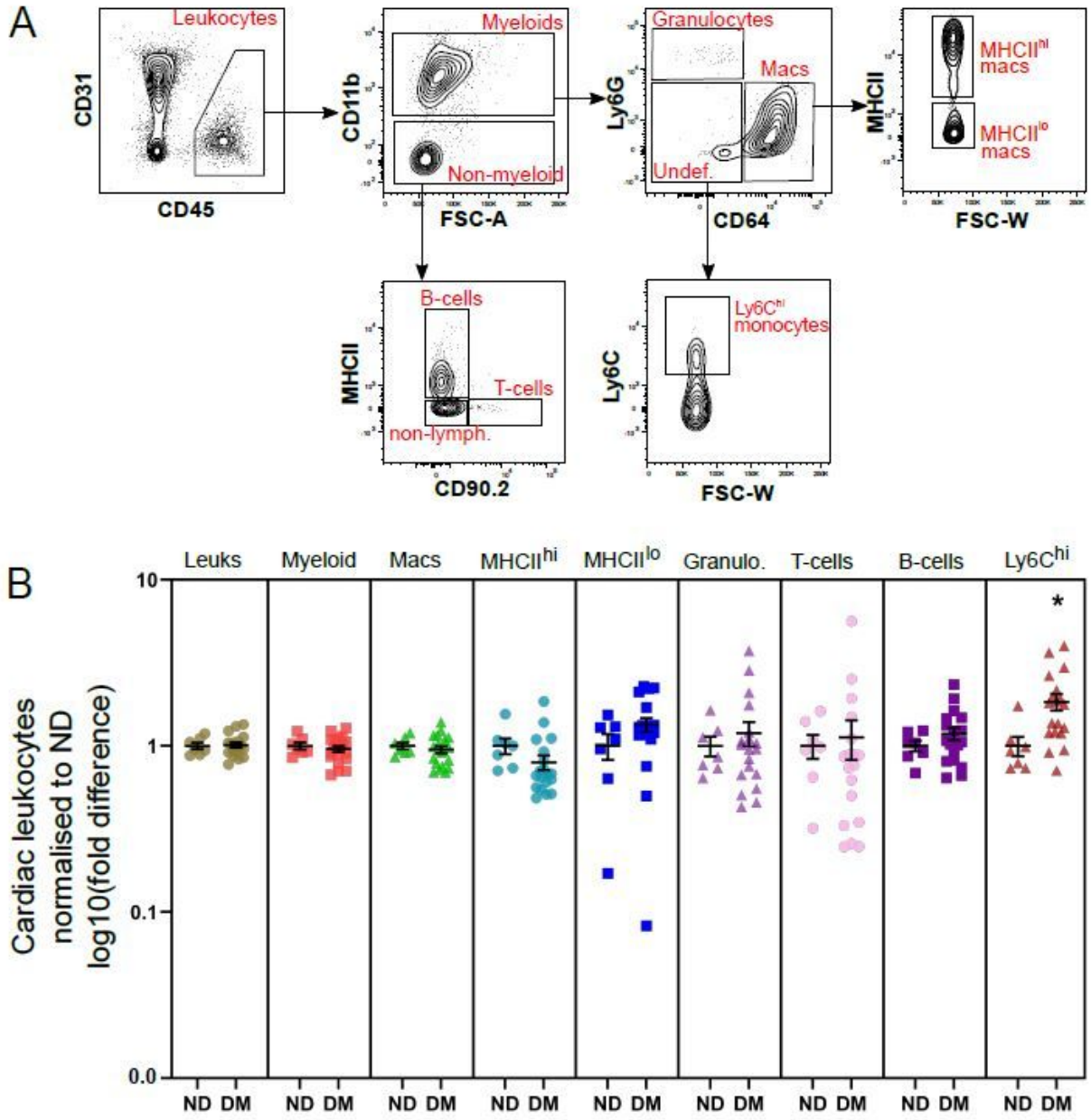

Figure 3

Ly6Chi monocytes, but not resident leukocytes are increased in the diabetic heart. (A) Flow cytometry contour plots display gating strategy for quantifying cardiac leukocytes (summarised in B). For full

gating strategy see Supplementary Figure 2. (B) Proportions of leukocyte sub-types in ND (n = 7) and T2D (n = 19) mouse ventricles. Data is displayed as mean ± SEM. *P < 0.05 (Student's unpaired t-test).

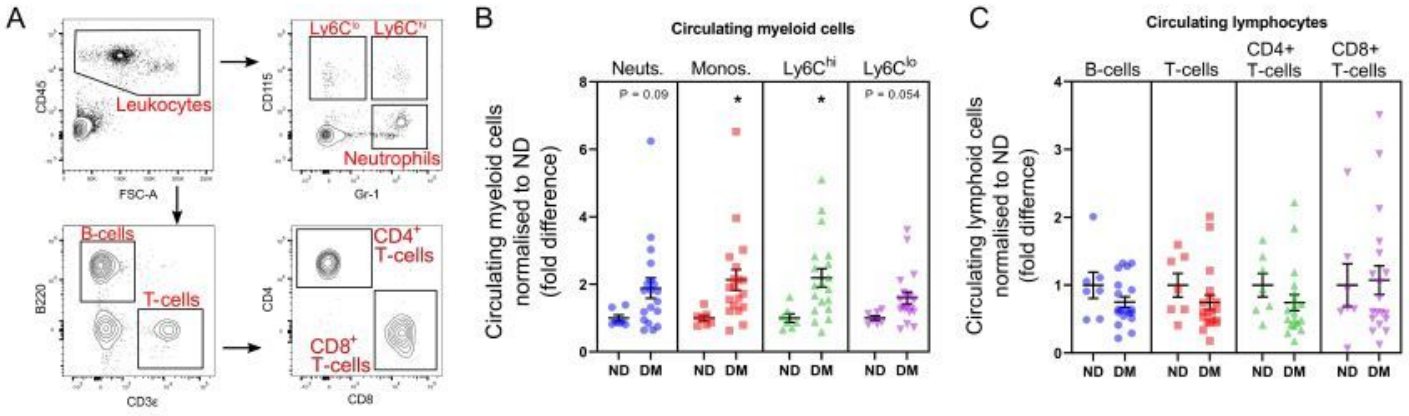

Figure 4

Mice with diabetes exhibit systemic monocytosis. (A) Flow cytometry contour plots display gating strategy for circulating leukocytes in whole blood (summarised in B and C). For full gating strategy see Supplementary Figure 2. (B-C) Proportions of circulating myeloid leukocytes and lymphocytes in ND (n = 7) vs. T2D (n = 19) mice. Monocytes (Monos.), Ly6Chi monocytes (Ly6Chi), Neutrophils (Neuts.) and Ly6Clo monocytes (Ly6Clo). Data is displayed as mean ± SEM. *P < 0.05 (Student's unpaired t-test).

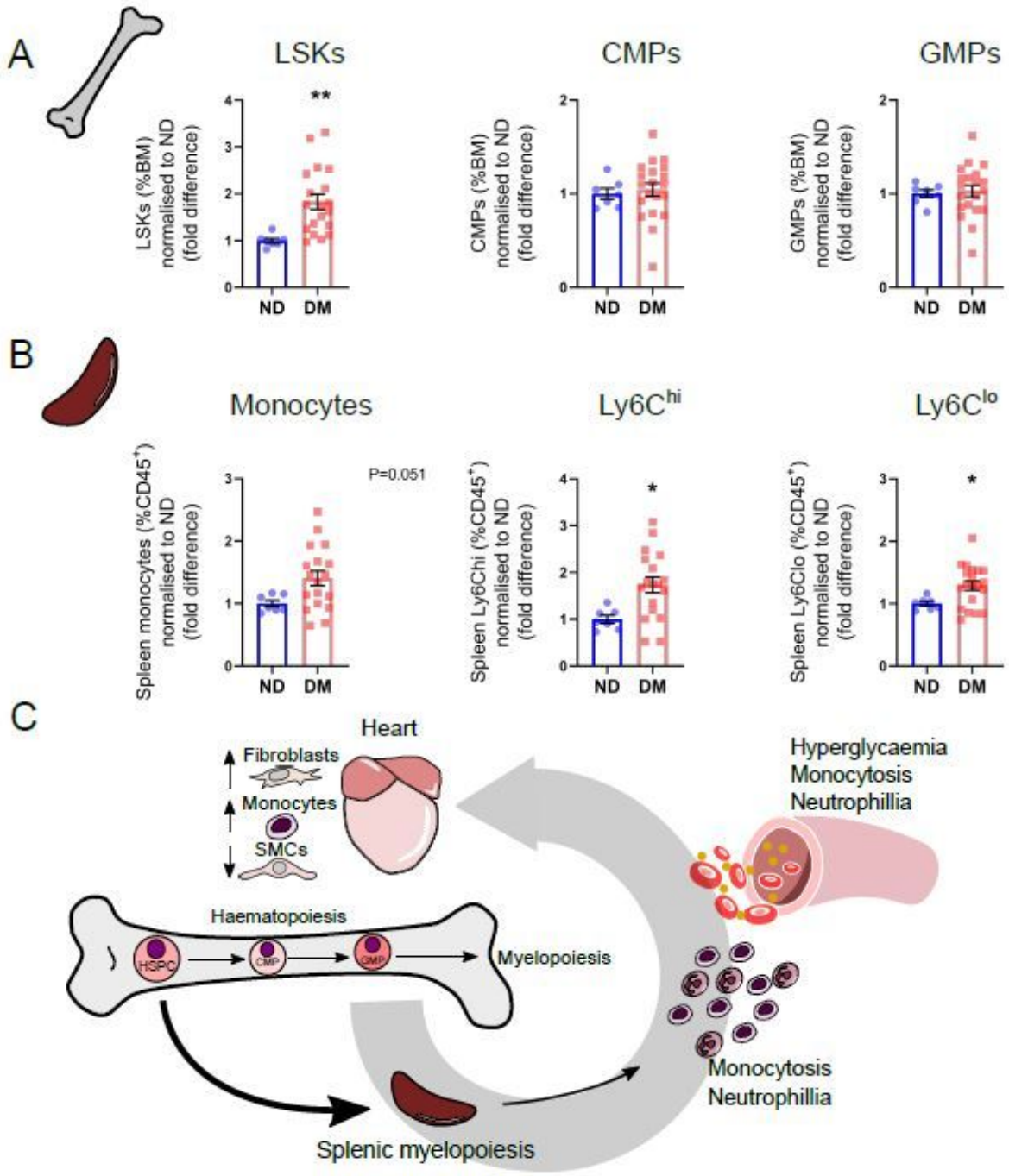

Figure 5

Bone marrow and spleen myelopoiesis evident in mice with diabetes. (A) Quantified proportions of bone marrow progenitor cells. LSK cells (Lineage-, Sca-1+, cKit+; haematopoietic stem cells), common myeloid progenitors (CMPs) and granulocyte myeloid progenitors (GMPs). (B) Proportions of spleen monocytes in ND (n = 7) vs. T2D (n = 19) mice. (C) Proposed mechanism by which systemic monocytosis occurs in diabetic mice administered STZ-HFD. See Supplementary Figure 4 and 5 for full gating strategies for flow cytometry analysis. Data displayed as mean ± SEM. *P < 0.05, **P < 0.01 (Student's unpaired t-test).

Supplementary Files

This is a list of supplementary files associated with this preprint. Click to download.

- CCOHENstzhfdcardiaccellularitySUPPcollated.pdf